Effect of Transverse Enthalpy Gradient on Blunt Body Pressure Distributions in Hypersonic Flow

DARRELL BROOKE* AND RICHARD E. THOMAS†
The Ohio State University, Columbus, Ohio

IT has been found that the flow produced in an arc-heated facility is likely to have transverse gradients in total enthalpy. Greenshields[1] measured average core gradients of the order of 81 Btu/lbm/in. in the Langley Field 2500-kw arc tunnel. An experimental investigation was conducted at The Ohio State University Aerodynamic Laboratory to determine whether a stream with transverse total enthalpy gradient was an acceptable medium for model pressure testing. The effect of total enthalpy gradient on the pressure distribution over a blunted 9° cone was investigated in a Mach 10 wind tunnel designed to produce enthalpy gradient flow. The results of this investigation are presented here. A more complete description of the experimental work may be found in Ref. 2.

Transverse total enthalpy gradients as high as 80 Btu/lbm/in. were induced in the test region of the 3-in. Mach 10 nozzle by the injection of unheated air along the nozzle wall upstream of the sonic throat. The strength of the induced gradient was dependent on the stagnation temperature of the air issuing from the heater and the mass fraction of unheated air injected into the nozzle. The enthalpy gradients were determined with a self-aspirating thermocouple temperature probe calibrated for local stagnation temperature in terms of measured temperature and impact pressure. Preliminary studies with the air injection nozzle are described in Ref. 3.

The model tested in the enthalpy gradient flow was a 9° blunted cone with nose to base radii in the ratio of one to four. The model, with five pressure orifices on the conical surface, was tested at zero angle of attack in flows having three different levels of enthalpy gradient as well as in flow with no gradient. Estimates of the possible measuring errors indicated that the probable error in the model pressure ratios should be less than ±4%. The model pressure ratios from all the model tests are compared in Fig. 1 using a representative zero gradient test as the reference. On the basis of this comparison, it must be concluded that the induced enthalpy gradients had no measurable effect on blunt body pressure ratios.

The nozzle surveys showed that there were negligible transverse Mach number gradients induced in the nozzle test region because of the enthalpy gradient. According to Newtonian impact theory, the pressure at a point on the body is

$$P = P_\infty + 2\, q_\infty \sin^2\theta$$

where P_∞ is the freestream static pressure, q_∞ is the freestream dynamic pressure, and θ is the angle of the surface relative to the flow direction. Since the Mach number across the core can be considered constant, it follows that P_∞ and q_∞ are also constant whether there is an enthalpy gradient or not. Thus, Newtonian theory predicts no effect of enthalpy gradient on the pressure distribution on the body. It should be noted that this simplified theory does not account for any rotational effects produced by the enthalpy gradients and that it is only applicable to "cold" flow and "frozen" flow where γ, the ratio of specific heats, can be considered constant across the core of the nozzle.

The results of the enthalpy gradient study indicate that the presence of large total enthalpy gradients across the test region will not significantly affect the pressure ratios obtained experimentally over a blunted body in cold or frozen flows. This result may not be applicable for sharp nosed bodies.

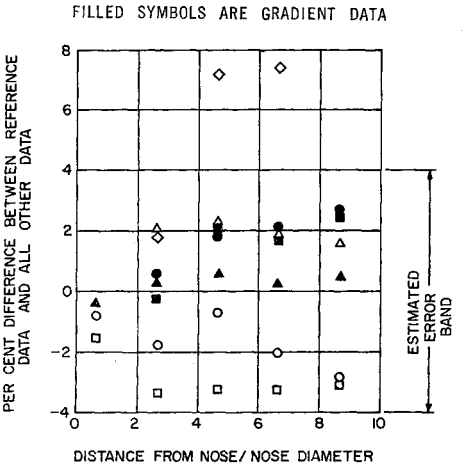

Fig. 1 Comparison of model pressure data.

References

[1] Greenshields, D. H., "Spectrometric measurements of gas temperatures in arc-heated jets and tunnels," NASA TN D-1960 (1963).

[2] Brooke, D. and Thomas, R. E., "The effect of wind tunnel enthalpy gradient on blunt body flows," Aeronautical Systems Div. Rept. (to be published).

[3] Petrie, S. L., "Investigations of co-axial air injection in a hypersonic wind tunnel," Aeronautical Research Lab., ARL 62-394 (August 1962).

Received May 28, 1964.

* Research Assistant, Department of Aeronautical and Astronautical Engineering.

† Assistant Supervisor, The Aerodynamic Laboratory. Member AIAA.

Air Ionization in the Hypersonic Laminar Wake of Sharp Cones

F. L. FERNANDEZ* AND E. S. LEVINSKY†
Aerospace Corporation, San Bernardino, Calif.

Introduction

THE principal sources of plasma generation in the flow field of a sharp slender re-entry body are the boundary layer and laminar wake.[1–5] This note compares the relative influence of these two sources of electron production on the re-entry radar observables. The authors have previously presented scaling laws for nonequilibrium ionization in the laminar boundary layer of sharp cones.[6] These scaling laws were based on a simplified model of clean air ionization kinetics and gave reasonable agreement with the more exact numerical solutions.[3, 5]

In the same spirit, scaling laws are developed herein for clean air ionization in the laminar wake. In lieu of available test data, an examination of the numerical laminar wake solutions of Lien et al.,[2] Li,[4] and Pallone et al.[7] shows that species diffusion and fluid entrainment are much weaker than in the laminar boundary layer with a catalytic wall and that the most important single parameter is the peak static enthalpy. The results also show that a nearly constant static enthalpy level is maintained along the wake centerline. Although the pressure in the laminar wake is approximately ambient, about one order below that on the cone, the com-

Received June 1, 1964. This work was supported by Ballistics Systems Division, U. S. Air Force, under Air Force Contract AF 04(695)-269.

* Member of the Technical Staff, Technology Division. Associate Member AIAA.

† Head, Gasdynamics Section, Technology Division. Member AIAA.

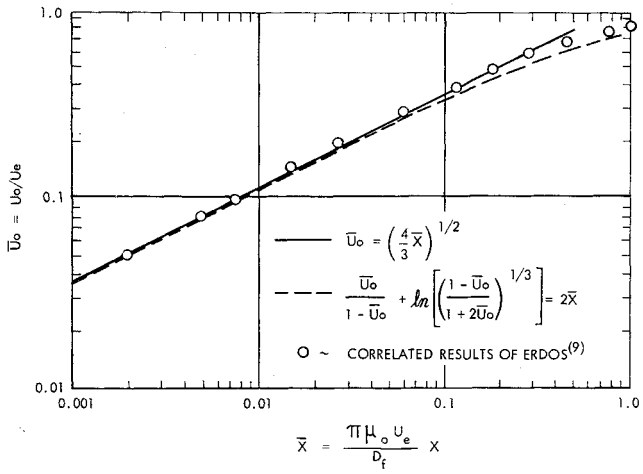

Fig. 1 Wake centerline velocity growth for slender cones.

pensating effects of long incubation periods (low velocity), small diffusion rates, small wake growth, elimination of the Mangler dilatant effect of the cone boundary layer,[6] and long running lengths all tend to increase electron production in the laminar wake with respect to that in the cone boundary layer. A relatively rapid decay in the centerline electron density is predicted following wake transition.[1, 4, 8] Thus, peak electron density levels should occur in the laminar wake or at the transition front.

In the following analysis, the flow is considered frozen at the boundary-layer composition in the free shear layer of the base flow region because of the rapid expansion. Electron production is restarted near the wake neck where the pressure rises to near ambient values. It is assumed that electrons are produced in the laminar wake until either local equilibrium ionization levels are reached or until wake transition occurs. The results of the approximate solutions are compared with the more exact calculations.[2, 7] Scaling laws for the effect of body size, shape, and altitude on wake electron production are given, and comparisons with boundary-layer electron density values are made for the assumption that peak wake and boundary-layer enthalpies are equal. It is recognized that the determination of the actual wake enthalpy

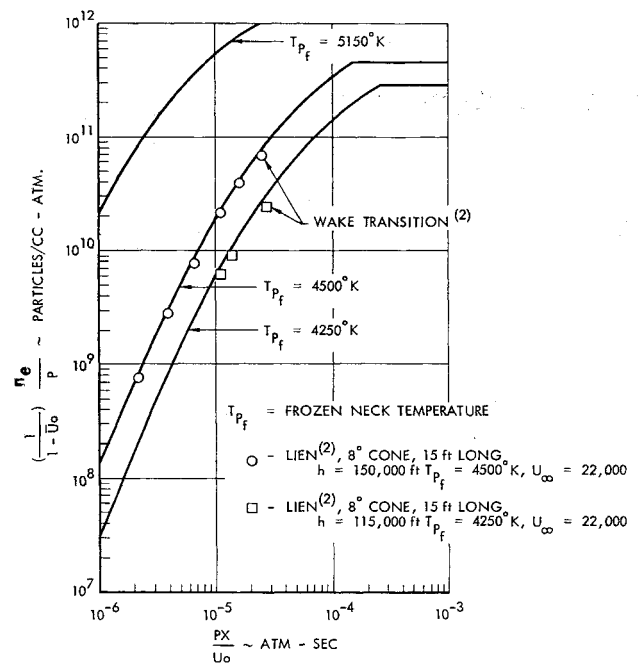

Fig. 2 Comparison of approximate solution with more exact results.

must await a detailed analysis of the base flow region and/or experimental wake surveys.

Discussion

For axisymmetric flow, neglecting pressure gradient terms and assuming binary diffusion with constant Schmidt number Sc, the conservation of species and momentum equations along the wake centerline become[7]

$$\rho_0 U_0 \frac{\partial C_{i0}}{\partial X} = \frac{2\mu_0}{Sc}\frac{\partial^2 C_i}{\partial r^2}\Big)_0 + \dot{w}_{i0} \tag{1}$$

$$\rho_0 U_0 \frac{\partial U_0}{\partial X} = 2\mu_0 \frac{\partial^2 U}{\partial r^2}\Big)_0 \tag{2}$$

where ρ_0, C_{i_0}, μ_0, and $\dot{w}_{i0}$ are the respective axis density, species mass fraction, viscosity, and species mass production rate per unit volume, X is the axial distance from the wake neck, and r the radial distance. Equations (1) and (2) may be integrated formally along the wake centerline if the species and velocity second derivatives are known and if the static temperature or enthalpy h_0 is given. Here h_0 is assumed constant along the wake centerline, based on the results of numerical calculations[2, 4, 7] wherein h_0 is found to be slowly varying and near the peak boundary-layer value, $h_0 \sim 0.3H_\infty$.

The two limiting cases of zero diffusion and of frozen chemistry across the wake are considered in evaluating the second derivative terms. Zero diffusion $Sc \to \infty$ leads to a streamtube analysis and should give the most rapid ionization on the wake centerline. For frozen chemistry across the wake, the species distributions across the wake are approximated by

$$\frac{C_i - C_{i_e}}{C_{i0} - C_{i_e}} = \left(\frac{1-\bar{U}}{1-\bar{U}_0}\right)^{Sc} \tag{3}$$

where $\bar{U} = U/U_e$, and the subscripts e and 0 refer to wake edge and centerline conditions, respectively. Equation (3) is readily shown to be valid in the frozen asympototic far wake and valid everywhere in the frozen wake for $Sc = 1$. Equation (3) should lead to minimal ionization rates along the wake centerline.

Neglecting diffusion, Eq. (1) may be integrated directly to

$$C_{i_0} = \frac{1}{U_e}\int_0^X \frac{\dot{w}_{i0}}{\rho_0}\frac{dX}{\bar{U}_0} + C_{i_0}(0) \tag{4}$$

On the other hand, Eqs. (1–3) can be combined to give

$$\frac{dC_{i0}}{dX} = \left(\frac{C_{i_e} - C_{i0}}{1-\bar{U}_0}\right)\frac{d\bar{U}_0}{dX} + \frac{\dot{w}_{i0}}{\rho_0}\frac{1}{\bar{U}_0 U_e} \tag{5}$$

Thus, Eq. (3) leads to a centerline species production rate explicitly independent of Schmidt number. For constant C_{i_e}, Eq. (5) integrates to

$$C_{i0} - C_{i_e} = (1-\bar{U}_0)\left\{\frac{1}{U_e}\int_0^X \frac{\dot{w}_{i0}}{\rho_0}\frac{dX}{\bar{U}_0(1-\bar{U}_0)} + C_{i0}(0) - C_{i_e}\right\} \tag{6}$$

Wake velocity growth

Consider again the momentum equation. Letting

$$\bar{Y}d\bar{Y} = \frac{1}{Y_N^2}\frac{\rho}{\rho_e}\left(\frac{r}{d}\right)d\left(\frac{r}{d}\right)$$
$$\frac{Y_N^2}{2} = \int_0^{r_e/d}\frac{\rho}{\rho_e}\left(\frac{r}{d}\right)d\left(\frac{r}{d}\right) \tag{7}$$

gives

$$\bar{U}_0\frac{d\bar{U}_0}{dX} = \frac{2\mu_0}{\rho_e U_e d^2}\frac{1}{Y_N^2}\frac{\partial^2\bar{U}}{\partial\bar{Y}^2}\Big)_0 \tag{8}$$

where d is the body diameter and r_e the wake radius. As-

suming that the velocity can be represented by a second-order polynomial in $\bar{Y}$ with boundary conditions

$$(\partial\bar{U}/\partial\bar{Y})\ (0) = 0 \qquad \bar{U}(0) = \bar{U}_0 \qquad \bar{U}(1) = 1$$

gives

$$(\bar{U} - \bar{U}_0)/(1 - \bar{U}_0) = \bar{Y}^2 \tag{9}$$

Equating momentum defect in the near wake to that contained in the boundary layer gives

$$[F_1(\bar{U}_0) - F_2(\bar{U}_0)]\rho_e U_e^2 Y_N^2 = D_f/2\pi d^2 \tag{10}$$

where

$$F_j = \int_0^1 \bar{U}^j \bar{Y} d\bar{Y}$$

and where D_f is the body friction drag. Equation (10) can be solved for Y_N^2 as a function of $\bar{U}_0$. Substitution into Eq. (8) gives

$$\frac{\bar{U}_0 d\bar{U}_0}{(1 - \bar{U}_0)dX} = \left(\frac{2}{3}\right)\frac{\pi\mu_0 U_e}{D_f}(1 + \bar{U}_0 - 2\bar{U}_0^2) \tag{11}$$

Equation (11) integrates to

$$\frac{\bar{U}_0}{1 - \bar{U}_0} + \ln\left[\left(\frac{1 - \bar{U}_0}{1 + 2\bar{U}_0}\right)^{1/3}\right] = 2\overline{X} \tag{12}$$

or, for small $\bar{U}_0$,

$$\bar{U}_0 \doteq (\tfrac{4}{3})^{1/2}\overline{X}^{1/2} \tag{13}$$

where

$$\overline{X} = (\pi\mu_0 U_e/D_f)X \tag{14}$$

Figure 1 is a plot of Eqs. (12) and (13). The parameter $\overline{X}$ is the same as that used by Erdos[9] to correlate exact numerical solutions, and the results of these numerical calculations are included in Fig. 1. The one-half power law, Eq. (13), gives reasonable agreement with detailed calculations for $\bar{U}_0 < 0.5$ and is used in the near wake analysis that follows. Consideration of higher-degree polynominals was found to offer little improvement when compared with Ref. 9 and cannot be substantiated because of the many assumptions already made. Both Eqs. (12) and (13) are in error for large $\bar{U}_0$, but it is expected that most electron generation in the laminar wake will occur at the lower velocities.

Laminar wake ionization

Using the simplified kinetics model,[6] the one-half power law for $\bar{U}_0$, and assuming constant temperature downstream from the neck, Eqs. (4) and (6) may be integrated directly giving

$$\frac{n_e}{P} = \frac{4.85 \times 10^{47} e^{-185{,}000/T}}{(T/1000)^{6.5}}\left(\frac{PX}{U_0/2}\right)^3 (1 - \bar{U}_0)^K \tag{15}$$

where K is 0 if species diffusion is neglected [Eq. (4)], K is 1 including species diffusion [Eq. (6)], and where T is in degrees Kelvin, P is in atmospheres, and X/U_0 has units of seconds. For small $\bar{U}_0$, diffusion is seen to play a relatively minor role, and $n_e/P \sim (PX/U_0)^3$ for a fixed temperature. It should be noted that Eq. (15) neglects the cooling effect of oxygen dissociation. This effect can be accounted for as discussed in Ref. 6. Figure 2 is a plot of Eq. (15) with the dissociative cooling correction for various initial temperatures (vibrational equilibrium). Included, also, are some results of Lien et al.[2]

Equation (15) can be used to compare electron production rates in the laminar near wake and the laminar boundary layer. For slender cone boundary-layer flows well out of equilibrium and neglecting species diffusion, it can be shown from Eq. (5) of Ref. 6 that

$$\frac{n_e}{P_\delta} = \frac{4.85 \times 10^{47} e^{-185{,}000/T}}{(T/1000)^{6.5}}\left(\frac{P_\delta X_\delta/3}{U_\delta/2}\right)^3 \tag{16}$$

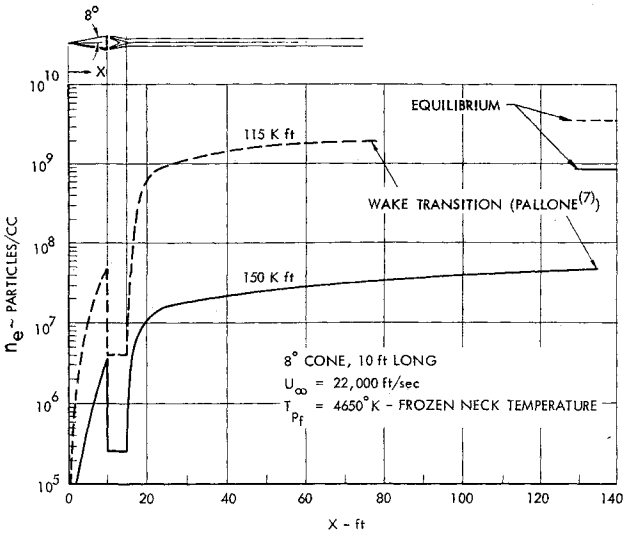

Fig. 3 Peak boundary-layer and wake electron concentrations.

where $U_\delta/2$ is the velocity in the boundary layer at peak temperature and $X_\delta/3$ the distance along the cone surface reduced for the Mangler effect.

Numerical results[6] indicate that boundary-layer diffusion decreases n_e/P_δ by a factor of about 30 for flows well out of equilibrium. Therefore, for the same peak neck and boundary-layer temperature,

$$\frac{n_{e\ \text{wake}}}{n_{e\ \text{boundary layer}}} \sim (27)(30)\left(\frac{P_e}{P_\delta}\right)^4\left(\frac{D_f}{2\pi\mu_0 U_e X}\right)^{3/2}\left(\frac{X}{X_\delta}\right)^3 \tag{17}$$

Considering a 10-ft, 8° cone at an altitude of 150,000 ft and velocity of 21,600 fps, and using the drag coefficients presented in Ref. 9, gives

$$\beta = \left.\frac{n_{e\ \text{wake}}}{n_{e\ \text{boundary layer}}}\right|_{X = X_\delta = 10\ \text{ft}} \approx 5 \tag{18}$$

Thus, for the same distance and initial temperatures, the peak electron levels reached in the near wake will be about one-half order of magnitude greater than those in the boundary layer. Thus, as pointed out by Lees,[1] the rapid rate of electron generation in the laminar near wake dominates the electron observables of slender bodies at high altitudes.

Equation (15) may be used to obtain scaling laws for laminar wake ionization since $\bar{U}_0 \sim (X/D_f)^{1/2}$. For geometrically similar cones, at a given set of flight conditions, $D_f \sim d^{3/2}$, so that at the same X/d behind the cones, $n_e \sim d^{15/4}$. In the boundary layer, $n_e \sim d^3$ so $\beta \sim d^{3/4}$ for similar bodies. On the other hand, since $D_f \sim \theta_c^2$ (Ref. 10) and in the boundary layer, $n_e \sim \theta_c^8$, $\beta \sim 1/\theta_c^5$, indicating that for increasing cone angle the laminar wake is much less important, provided peak temperatures in the neck and boundary layer remain comparable. Of course, for large θ_c, the inviscid flow field will dominate electron production. At different altitudes, as long as equilibrium is not approached, $\beta \sim P^{3/4}$.

It can be concluded, therefore, that at the same x/d in the laminar wake, $\beta \sim (Pd)^{3/4}$, as long as equilibrium is not approached, viz., binary scaling.

Finally, Fig. 3 presents a calculation performed on an 8° cone at 115 and 150 kft, assuming the peak neck and boundary-layer temperatures are equal. The electron production in the boundary layer and wake is shown, and the relative rapidity of wake electron generation is demonstrated.

References

[1] Lees, L., "Hypersonic wakes and trails," AIAA J. 2, 417–428 (1964).

[2] Lien, H., Erdos, J., and Pallone A., "Nonequilibrium wakes with laminar and turbulent transport," AVCO Rept. RAD-TM-63-87 (January 22, 1964).

[3] Blottner, F. G., "Nonequilibrium laminar flow of ionized air," AIAA Preprint 64-41 (January 1964).

[4] Li, H., "Study of hypersonic contaminated wake by an exact numerical solution," General Electric Co. Rept. MSD-R63SD63 (December 1963).

[5] Pallone, A., Moore, J., and Erdos, J., "Nonequilibrium nonsimilar solutions of the laminar boundary layer equations," AIAA Preprint 64-40 (January 1964).

[6] Levinsky, E. S. and Fernandez, F. L., "Approximate nonequilibrium air ionization in hypersonic flows over sharp cones," AIAA J. 2, 565–568 (1964).

[7] Pallone, A. J., Erdos, J. I., Eckerman, J., and McKay, W., "Hypersonic laminar wakes and transition studies," AIAA Preprint 63-171 (June 1963).

[8] Webb, W. H. and Hromas, L. A., "Turbulent diffusion of a reacting wake," AIAA Preprint 64-42 (January 1964).

[9] Erdos, J. and Pallone, A., "Correlation of numerical solutions of the laminar wake," AIAA J. (submitted for publication).

[10] Hromas, L. A. and Lees, L., "Effect of nose bluntness on the turbulent hypersonic wake," Space Technology Lab. Rept. BSD-TDR-62-354 (October 1962).

Asymmetrical Buckling of Spherical Caps under Uniform Pressure

GAYLEN A. THURSTON*
Martin-Marietta Company, Denver, Colo.

Nomenclature

a = radius of curvature of shell
E = Young's modulus
H = height of shell center above plane through the edge
w = normal displacement of shell midsurface
N_θ = circumferential average stress
h = shell thickness
n = number of circumferential waves in buckling mode
ν = Poisson's ratio
λ = geometrical parameter $= 2[3(1-\nu^2)]^{1/4}(H/h)^{1/2}$
q = uniform normal pressure
q_{cr} = buckling pressure
q_0 = classical buckling pressure of complete spherical shell $= 2Eh^2/a^2[3(1-\nu^2)]^{1/2}$
p = buckling pressure ratio $= q_{cr}/q_0$

SEVERAL investigators have explored the possibility that accurate buckling loads for shells of revolution under axisymmetric loads can be obtained by computing axisymmetric equilibrium positions using nonlinear finite deflection theory and then checking these equilibrium states for points of bifurcation into asymmetric buckling modes that differ from the prebuckled modes by infinitesimal amounts. The buckling criterion is the same as in classical bifurcation theory, but the assumption of the linearized theory that the prebuckled state of stress can be represented by membrane theory has been discarded. Stein[1a] has used this approach to compute the effect of simply supported edges on the stress distribution and buckling loads of cylinders under axial compression and uniform pressure. Huang,[2] Weinitschke,[1b] and Parmerter and Fung[1c] have studied the asymmetric buckling of clamped shallow spherical shells under uniform pressure.

Table 1 Calculated buckling pressures p

λ	n	This note	Huang[5]
6	2	0.777	0.775
	3	0.814	0.827
	1	0.943	0.919
8	4	0.756	0.766
	3	0.778	0.774
	2	0.886	0.893
12	7	0.789	0.780
	8	0.794	0.790
	6	0.804	0.798
16	10	0.789	0.792
	12	0.803	0.800
	11	0.810	0.790
20	15	0.806	...
	16	0.806	...
	17	0.826	...

Received June 3, 1964.
* Associate Research Scientist.

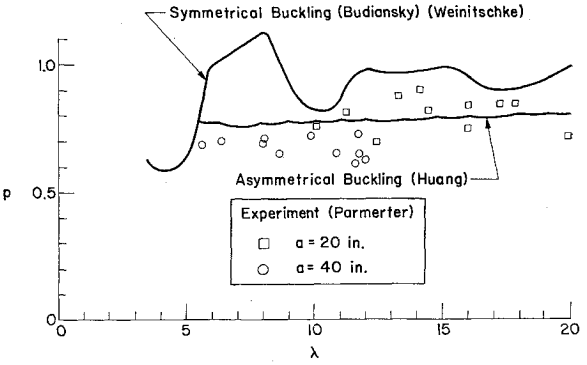

Fig. 1 Stability curves compared with Parmerter's experimental results.

This note presents buckling pressures for spherical caps obtained from a digital computer program[3] that is based on the same type of analysis as the forementioned references but is applicable to general shells of revolution. The program computes buckling stresses due to external pressure, axial load, torsion and axisymmetric temperature gradients, or combinations of these. It can also compute natural frequencies of free vibration of shells under all of these loads except torsion.

This solution is restricted to thin isotropic shells of revolution. The thickness and Young's modulus of the shell can vary continuously in the meridional direction, but not in the circumferential direction. The boundary conditions can be any linear combination of stress resultants and deflections.

The buckling pressures for clamped spherical caps reported by Huang do not agree with those of Weinitschke. Parmerter[4] has obtained results for a limited range of λ that agree with Huang's results. Table 1 lists buckling pressures from the present computer program and corresponding data from Huang's report.[5] Huang's results are from shallow-shell theory, whereas the pressures in this note are from a more general theory with a semiapex angle of the shell of 11.5°; both sets of calculations used $\nu = \frac{1}{3}$. The results of the two theories show good agreement.

Figure 1 shows the envelope of Huang's buckling pressures plotted as a function of λ along with some recent experimental results reported by Parmerter and the curve for axisymmetric snap buckling obtained by Budiansky[6] and by Weinitschke.[7]

Parmerter's experimental pressures are for near perfect shells and some are actually higher than the theoretical curve for bifurcation buckling, although they lie below the theoretical curve for snap buckling. A tentative explanation could be that the asymmetric post-buckling equilibrium states are stable at pressures near the bifurcation point. For large values of λ, the axisymmetric hoop stress and the asymmetric normal deflection mode shape attain their maximum values near the clamped boundary† (see Fig. 2). It is possible that the clamped spherical cap can wrinkle near the edge in a manner analogous to that of rectangular plates in compression. A confirmation of this assumption would require actual asymmetric solutions of the finite deflection equations for spherical

† Huang[5] derives an asymptotic solution for the boundary-layer effect on the mode shape.